**Theoretical Model of the Actuator**

To precisely characterize the performance of the PSE, we developed analytical models for the geometry and physical principles of both the bending and deployable actuators. These models explicitly describe the relationship between the input (internal air pressure, P) and the key performance outputs (kinematics and static forces).

**Bending Actuator Model**

The bending actuator is constructed from N individual bladder units serially connected along a non-extensible fabric base. Bending motion is achieved by pressurizing the bladders; the resulting pressure on the internal top surface generates the actuation torque.

**A. Kinematic Model**

We first analyze the geometry of a single bladder unit. Based on experimental characterization, both the bending height $h_1$ and the change in width $\Delta w_1$ of a single unit are nonlinear functions of the internal air pressure P, expressed as:

$$\begin{aligned} h_1 &= f_h(P) \\ \Delta w_1 &= f_w(P) \end{aligned} \tag{1}$$

Following the kinematic model illustrated in Fig. S1, the local bending angle $\theta_0$ contributed by a single bladder unit can be expressed as:

$$\theta_0 = 2ar\tan(\frac{h_1}{w_1 + c + \alpha\Delta w_1}) \tag{2}$$

Here, $w_1$ is the initial width of the bladder, $c$ is the distance between adjacent bladders, and $\alpha$ is a non-linear scaling coefficient for the width change. For an entire bending actuator composed of $N$ such units, the total bending angle $\theta_z$ is the linear superposition of the contribution from each unit:

$$\theta_z = N2ar\tan(\frac{h_1}{w_1 + c + \alpha\Delta w_1}) \tag{3}$$

**B. Static Torque Model**

Assuming a uniform internal pressure $P$, the pressure acts on the effective internal area of each bladder, $S_{eff}$, generating a vertical force, $F_{seg}$.

$$F_{seg}(P) = PS_{eff} \tag{4}$$

The effective area $S_{eff}$ is approximated by the area of a single bladder unit, where the length of each bladder is $l_{eff}$. The torque of the actuator can then be expressed as:

$$\tau_z = NPl_{eff} \tag{5}$$

**Deployable Actuator Model**

The deployable actuator generates an antagonistic resistive torque, $\tau_{GH}$, by deploying and applying a supportive force, $F_{sup}$, to the upper arm.

**A. Kinematic Model**

As shown in Fig. S1, the deployment angle of the actuator can be derived as:

$$\theta_{abd-Fro}(P) = 2Mar\tan(\frac{h_2}{w_2 + \Delta w_2}) \tag{6}$$

where $M$ is the number of bladder units.

## B. Static Torque Model

The interaction area of the deployable actuator is defined by the contact surfaces at its two distal ends (with the torso and the upper arm).

$$S_{sup} = 2h_2 l_2 \tag{7}$$

When pressurized with an internal pressure $P$, the actuator produces a supportive force $F_{sup}$:

$$F_{sup}(P) = Ph_2 l_2 \tag{8}$$

Consequently, the supportive torque generated at the glenohumeral joint is:

$$\tau_{GH} = Ph_2 l_2 l_{arm} \tag{9}$$
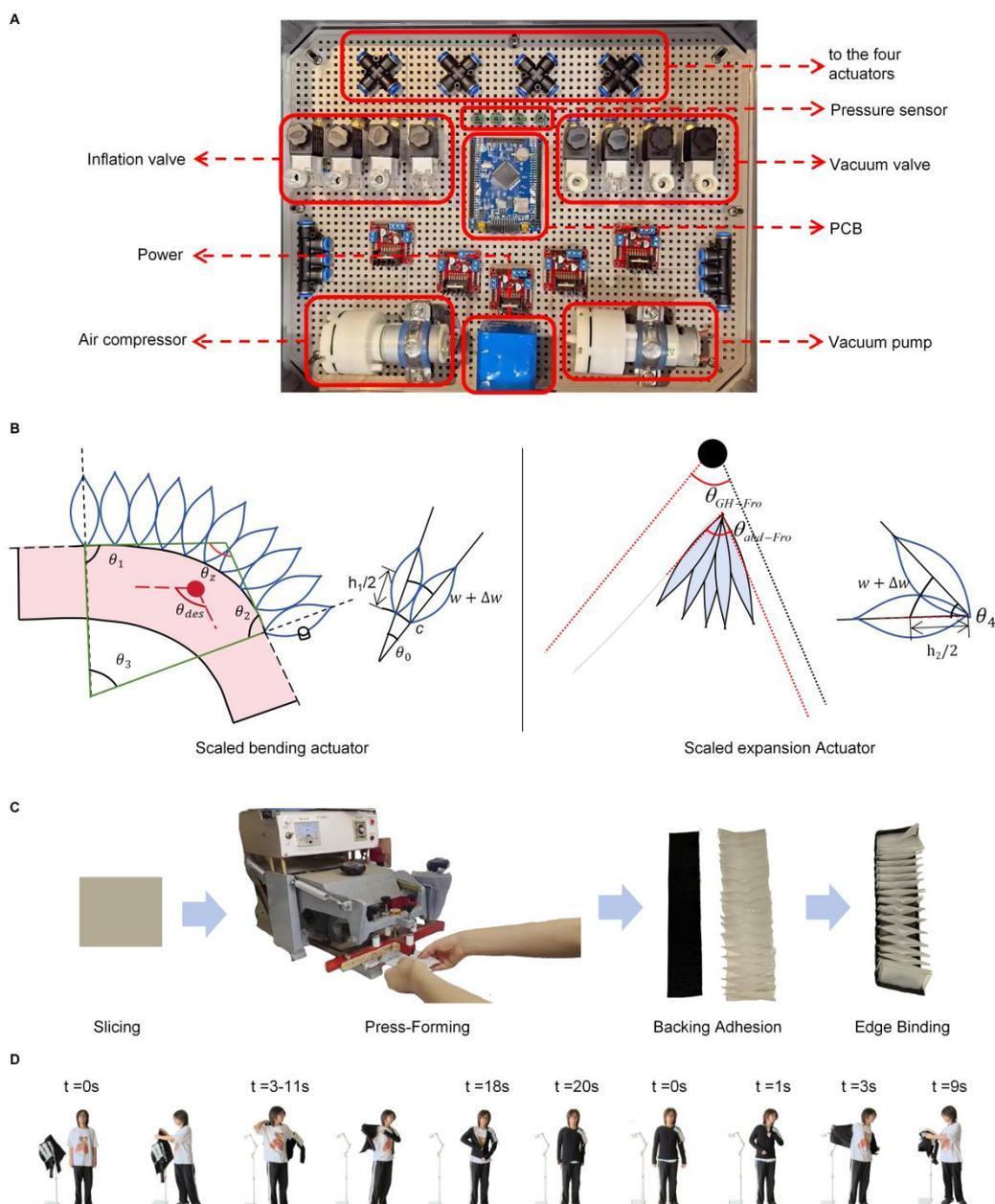
**Supplementary Figures:**



**Fig. S1. Component details of PSE.** (**A**) PSE Hardware System. (**B**) Kinematic design of the scaled bending actuator and the scaled deployable actuator. (**C**) Fabrication workflow of the actuators: slicing of coated fabric sheets, press-forming of the pouch array using a heat press, bonding a backing layer, and edge binding to obtain the final actuator module ready for integration. (**D**) Donning/doffing sequence for the wearable system. Representative time stamps illustrate the quick procedure to wear, secure, and remove the device.
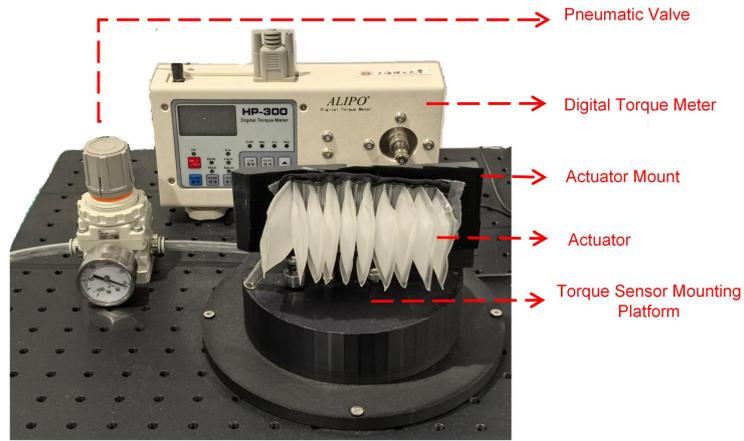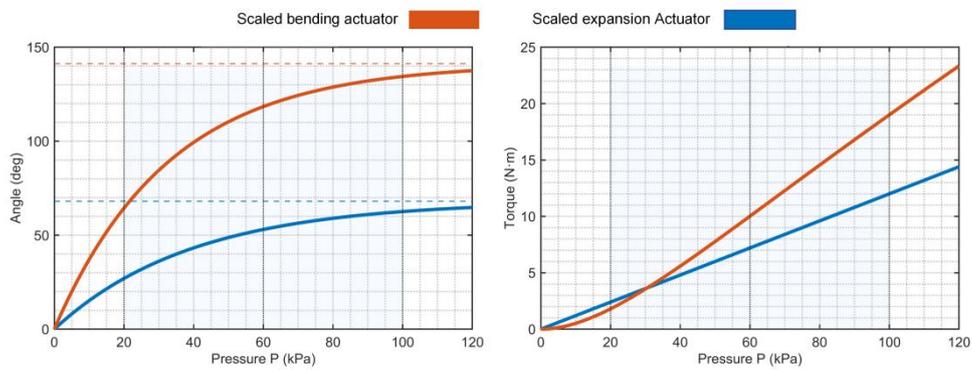
**Fig. S2. The torque measurement platform**



**Fig. S3. Angle and torque versus internal pressure for scaled bending and deployable pneumatic actuators.** (**A**) Angle as a function of internal pressure for the scaled bending actuator (blue) and the scaled deployable actuator (orange). (**B**) Output torque as a function of internal pressure.

**Table S1. Testing participant population**

| ID | Sex (as assigned at birth) | Height (m) | Weight (kg) |
|----|------|------|------|
| 1 | F | 1.60 | 50 |
| 2 | M | 1.68 | 65 |
| 3 | M | 1.65 | 50 |
| 4 | F | 1.7 | 55 |
| 5 | M | 1.73 | 65 |
| 6 | M | 1.72 | 50 |
| 7 | F | 1.77 | 60 |
| 8 | M | 1.83 | 73 |
| 9 | M | 1.75 | 85 |
| 10 | M | 1.73 | 67 |

**Table S2.   Participants in user assessment**

| ID | Sex (as assigned at birth) | Height (m) | Weight (kg) | Muscle Strength Grade |
|----|----------------------------|------------|-------------|-----------------------|
| 1 | M | 1.72 | 74 | 3 |
| 2 | F | 1.51 | 60 | 2+ |
| 3 | M | 1.8 | 76 | 3 |
| 4 | M | 1.76 | 70 | 4 |
| 5 | F | 1.52 | 55 | 4 |
| 6 | F | 1.55 | 50 | 4 |
| 7 | M | 1.65 | 68 | 4 |

**Table S3. Summary of trajectory tracking errors (RMSE) across all participants**

| Condition | RMSE_X/mm | RMSE_Y/mm | RMSE_Z/mm | RMSE_Total/mm | Mean 3D Distance/mm |
|-----------|-----------|-----------|-----------|---------------|---------------------|
| 0 | 9.42 | 9.52 | 14.99 | 20.17 | 15.38 |
| 1 | 3.42 | 5.76 | 9.96 | 12.01 | |
| 0 | 17.18 | 21.70 | 10.09 | 29.46 | 45.78 |
| 1 | 15.07 | 36.03 | 8.39 | 39.95 | |
| 0 | 9.77 | 22.75 | 6.81 | 25.92 | 28.92 |
| 1 | 7.03 | 10.70 | 3.48 | 13.27 | |
| 0 | 24.37 | 31.54 | 12.42 | 42.24 | 28.31 |
| 1 | 23.84 | 27.46 | 14.58 | 39.18 | |
| 0 | 12.38 | 14.31 | 20.23 | 28.53 | 18.52 |
| 1 | 7.09 | 9.10 | 14.80 | 18.77 | |